Hindawi
Advances in Civil Engineering
Volume 2021, Article ID 9998545, 9 pages
https://doi.org/10.1155/2021/9998545

Research Article

Height of the Fractured Zone in Coal Mining under Extra-Thick Coal Seam Geological Conditions

Dequan Sun,[1,2] Xiaoyan Li,[1,2] Zhijie Zhu ,[1,3] Yang Li,[1,2] and Fang Cui[1,2]

[1]*Engineering Laboratory of Deep Mine Rockburst Disaster Assessment, Jinan 250104, China*
[2]*Shandong Provincial Research Institute of Coal Geology Planning and Exploration, Jinan 250104, China*
[3]*Mining Engineering School, Liaoning Technical University, Fuxin 12300, China*

Correspondence should be addressed to Zhijie Zhu; zhuzhijie@lntu.edu.cn

Received 30 March 2021; Accepted 29 July 2021; Published 11 August 2021

Academic Editor: Hui Yao

Copyright © 2021 Dequan Sun et al. This is an open access article distributed under the Creative Commons Attribution License, which permits unrestricted use, distribution, and reproduction in any medium, provided the original work is properly cited.

The height of the fractured zone caused by coal mining is extremely significant for safely mining under water, water conservation, and gas treatment. At present, the common prediction methods of overburden fractured zone height are only applicable to thin and medium-thick coal seams, not suitable for thick and extra-thick coal seams. In order to determine the overburden fractured zone distribution characteristics of extra-thick seam mining, failure process analysis method of overlying strata was proposed based on key strata theory. This method was applied to 15 m coal seam of Tongxin coal mine, and fractured zone height was determined to be 174 m for 8100 panel. EH4 electromagnetic image system and borehole televiewer survey were also conducted to verify the theory results. The distribution of the electrical conductivity showed that the failure height was 150–170 m. Observation through the borehole televiewer showed that the fractured zone height was 171 m. The results of the two field test methods showed that the fractured zone height was 150–171 m, and it was consistent with the theory calculation results. Therefore, this failure process analysis method of overlying strata can be safely used for other coal mines.

1. Introduction

The deformation and failure are changed by the mining process. After coal is mined out, overlying strata will deform and break, and the overlying strata can be classified to caved zones, fractured zones, and continuous bending zones. The fractures formed in the overburden are the channels for mine water inrush. Thus, the development process of fractures in the overburden is the basis for determining the occurrence, and predicting and formulating control measures for mine water inrush [1]. At the same time, in order to properly lay out the mine and to efficiently drain the methane gas, it is also extremely important to accurately determine the fracture characteristics of the overburden [2, 3]. At present, the commonly used guide height prediction methods in my country are the empirical formulas given in the ≪Code for Building, Water, Railway, and Main Roadway Coal Pillar Setting and Compression Coal Mining≫, but these formulas are only applicable to thin coal seams and medium-thick coal seams. For thick and extra-thick coal seams, there is no suitable theory for determining overlying failure height.

Some scholars at home and abroad have conducted a lot of research on the failure height of thick coal seams. Liu et al. studied overburden failure characteristics in deep thick loose seam and thick coal seam mining [4]. Wang al. used microseismic monitoring system, ground penetrating radar, and borehole televiewer system, and the height of water flowing fractured zone of fully mechanized top caving was monitored [5]. van Schoor applied in-mine electrical resistance tomography (ERT) to map potholes and other disruptive features ahead of mining [6]. Kidybinski and Babcock used a two-dimensional finite element method of stress analysis to study the development of the fracturing process within the roof rock of a longwall face in a coal mine [7]. Palchik studied the fractured zones caused through the change in natural gas emission during longwall coal excavation [8]. Mills et al. measured shear movements in the

overburden strata ahead of longwall mining [9]. Ju et al. studied the effect of sand grain size on simulated mining-induced overburden failure in physical model tests [10]. Sun et al. used distributed optical fiber sensing to detect overburden deformation and failure in a mining face [11]. Application of magnetotelluric method to the detection of overburden failure height in shallow seam mining is done [12]. Chen et al. used RFPA software to simulate the whole process of overburden deformation and caving during mining and determined the fractured zone height [13]. Wang applied microseismic monitoring method to determine the fractured zone height [14]. Wang et al. studied the process of overburden failure in steeply inclined multiseam mining: insights from physical modelling [15]. Liu et al. used numerical simulation software FLAC3D to investigate overburden failure characteristics in deep thick loose seam and thick coal seam mining [4]. Xu et al. analyzed the overburden migration and failure characteristics after mining shallow buried coal seams with thick loose layer based on actual measurement data and simulation results [16]. Peng et al. analyzed main controlling factors of overburden failure in coal mining under thick coal seam geological conditions [17]. Yang et al. studied the evolution characteristics of two-zone failure mode of the overburden strata under shallow buried thick seam mining using physical modelling and on-site observation [18]. Judging from the research progress at home and abroad, few people have established mechanical model of overlying rock structure to analyze the overburden failure height.

In this paper, 8100 panel of Tongxin coal mine in China was selected as a research object. Failure process analysis method of overlying strata was proposed based on key strata theory. EH4 electromagnetic image system and borehole televiewer survey were conducted to verify the theory results. The results can provide a guidance for mining safety and economy.

2. Geology and Mining Conditions

The Tongxin Minefield is located in the north east of the Datong Coalfield, China, and it belongs to the east wing of the Datong syncline. The basic structure is a monoclinic structure that strikes N10~55°E, tendency northwest, high in the east and low in the west. The stratum dip is generally 3–10°. In the southeast and the south, the stratum dip near the coal seam outcrop is steep, generally 30–80°, and it is upright and inverted locally. The dip angle of the formation to the northwest quickly becomes flat. The mine field structure is simple. There are few faults in the minefield, and there are two normal faults. The faults are spread along the NNE direction and tend to the northwest. There are two larger folds in the minefield, namely, the Diaowozui syncline and the Hanjiayao anticline, and there are second-order small folds associated with them.

Panel 8100 of No. 3–5 seam was selected for this study. Its average thickness was 15.3 m, and the dip is 2°~3°. The thickness of the coal seam varies a little. The roof strata above No. 3–5 seam are shown in Table 1, and hard strata account for a large part. The panel width along the dip direction was 193 m, and the panel length along the strike direction was 1406 m. The top coal caving method was used to extract the full seam thickness with mining height 3.9 m at the bottom of the seam and the remaining 11.4 m on the top by natural caving. The gob of No. 14 seam located 190 m above the No. 3–5 seam covered about half of the panel length. The width of the section coal pillar was 38 m, and the speed of mining face was 5.6 m every day. Shield type low-level top coal caving hydraulic support was used in this longwall face, and its type was ZF15000/27.5/42.

3. Determination of Failure Height of Overlying Strata Based on Key Strata Theory

3.1. Determination of Key Strata. For the hard roof group structure with different thickness, the bearing capacity of the roof of each stratum should be clarified to determine the bearing capacity of the roof group structure. The bearing capacity of the multistrata roof composite structure satisfies the following relationship [19, 20]:

$$(q_n)_m = \frac{E_m h_m^3 \sum_{i=m}^{n} h_i \gamma_i}{\sum_{i=m}^{m} E_i h_i^3}, \tag{1}$$

where $(q_n)_m$ is the load imposed by the roof of the nth stratum on the roof of the mth strata; m, n, $i$are No. of roof rock stratum; E_m is the elastic modulus of the mth strata MPa; h_m, h_i are the thickness of the mth strata and the ith strata, m; γ_i is the volume-weight of the ith strata kN/m^3.

In the process of deformation of the key strata, simultaneous deformation happens to the overlying strata controlled, while the lower strata are not deformed. Thus, the load it bears no longer needs to be borne by the lower rock. If the nth strata are the roof of the key strata, the following relationship shall be satisfied [21, 22]:

$$(q_n)_m < \left(q_{(n-1)}\right)_m, \tag{2}$$

where $(q_n)_m$ is the load kNimposed by the nth strata on the mth strata; $(q_{(n-1)})_m$ is the load kNimposed by the $(n-1)$strata on the mth strata.

At the same time, the key strata need to meet the strength conditions. If the failure span of the lower hard stratum is less than that of the upper hard stratum, the strength criterion of the key strata is [23]

$$l_{(n+1)} > l_1, \tag{3}$$

where $l_{(n+1)}$is the failure span of the $n+1$strata, m; $l_1$is the failure span of the lth strata, m.

3.2. Failure Process Analysis of Upper Overlying Strata. Fixed beam mechanical model is used to estimate limited span of hard stratum [24]:

$$l_G = h\sqrt{\frac{2\sigma_t}{q}}, \tag{4}$$

where $h$is the thickness of the strata, $\sigma_t$is the ultimate tensile strength of the strata, and $q$is the strata load.

Table 1: Characteristics of overlying strata.

No.	Lithology	Elastic modulus (GPa)	Tensile strength (MPa)	Bulk force (kN/m^3)	Thickness (m)
1	Sandy mudstone	18.35	5.47	26.31	3.2
2	K3 sandstone	36.21	7.68	25.44	5.3
3	Medium sandstone	29.57	6.14	26.73	7.7
4	Fine sandstone	35.54	7.81	27.12	2.1
5	Siltstone	23.64	4.97	26.45	5.3
6	4 coal	4.20	1.27	10.36	2.1
7	Siltstone	23.35	4.25	25.78	2.4
8	Kernstone	20.32	4.82	24.21	4.3
9	Fine sandstone	35.62	8.20	25.62	14.8
10	Conglomerate	28.43	4.34	27.35	12.9
11	Kernstone	19.98	5.24	23.89	3.5
12	Conglomerate	28.74	4.34	27.10	12.0
13	Medium sandstone	29.62	7.01	25.52	13.7
14	Siltstone	23.48	4.45	24.58	3.2
15	Fine sandstone	35.21	7.93	27.17	10.7
16	Conglomerate	28.64	4.23	26.95	4.6
17	Fine sandstone	36.01	7.87	26.51	10.3
18	Siltstone	23.17	4.52	25.20	10.5
19	Sandy mudstone	18.46	5.81	25.98	6.9
20	Conglomerate	28.42	3.92	27.15	5.1
21	Sandy mudstone	18.56	4.14	26.51	2.9
22	Fine sandstone	36.12	8.11	26.82	10.7
23	Kernstone	21.31	5.34	25.24	14.3
24	Fine sandstone	35.87	8.64	27.54	6.2
25	Kernstone	20.12	5.42	25.37	25.4

For the weak strata, the limited span at the maximum horizontal tensile strain [25] is

$$l_R = h\sqrt{\frac{8E\varepsilon_{\max}}{3q}}, \tag{5}$$

where $E$is the elastic modulus of the strata, and $\varepsilon_{\max}$is the maximum horizontal tensile strain of the strata.

The maximum deflection of the weak strata [25] is

$$\omega_{\max} = \frac{5ql^4}{384EI}, \tag{6}$$

where $l$is the limited failure span of the rock strata; $I$is the moment of inertia of the section.

The free space height underneath the rock strata [26] is

$$\Delta_i = M - \sum_{j=1}^{i-1} h_j\left(k_j - 1\right), \tag{7}$$

where $\Delta_i$is the free space height underneath the ith strata; $M$is the coal seam mining height; $h_j$is the thickness of the jth strata; $k_j$is the residual frosting coefficient of the jth strata.

The critical mining length at failure [27, 28] is

$$L = \sum_{i=1}^{m} h_i \cot\ \varphi_q + l + \sum_{i=1}^{m} h_i \cot\ \varphi_h, \tag{8}$$

where: $m$is the number of strata between coal seam roof and the lower part of the strata; $h_i$is the thickness of the ith strata; $\varphi_q$and $\varphi_h$are the front and rear fracture angles of the strata, respectively.

The overlying strata failure process is affected by the tensile strength of the key strata, the antistrain ability of the soft rock strata, the free space height beneath the rock formation and the propulsion distance of the working face, etc. The evolvement of overlying strata failure can be judged by the relationship between the failure of key strata and the soft rock and the free space height beneath them. Specific judgments are shown in Figure 1.

3.3. Analysis of Overlying Strata Failure of Tongxin Coal Mine. Since the Jurassic mined-out area is located about 190 m above the 8100 working face, the calculated scope of the key strata ends with the Jurassic mined-out area. There are 25 strata between the 8100 working face and the Jurassic coal seam, among which hard sandstone and conglomerate predominate. According to identification conditions of the key strata, each key stratum of overlying strata above the 8100 working face is identified combined with formulas (1)–(3), with the results shown in Table 2.

According to the identification results of the key strata and the identification formulas (4) to (8), and according to the overlying strata failure height identification process (Figure 1), the development of overlying strata failure is determined (Table 3), when the working face advanced to different positions. It can be seen from the table that the inferior key strata I and the inferior key strata II are broken when the working face advances to 55 m and 109 m, and the controlled strata above them are destroyed. Overlying strata have a failure height of 32 m and 143 m. When the face is advanced to 193 m, the key strata III are broken. Overlying

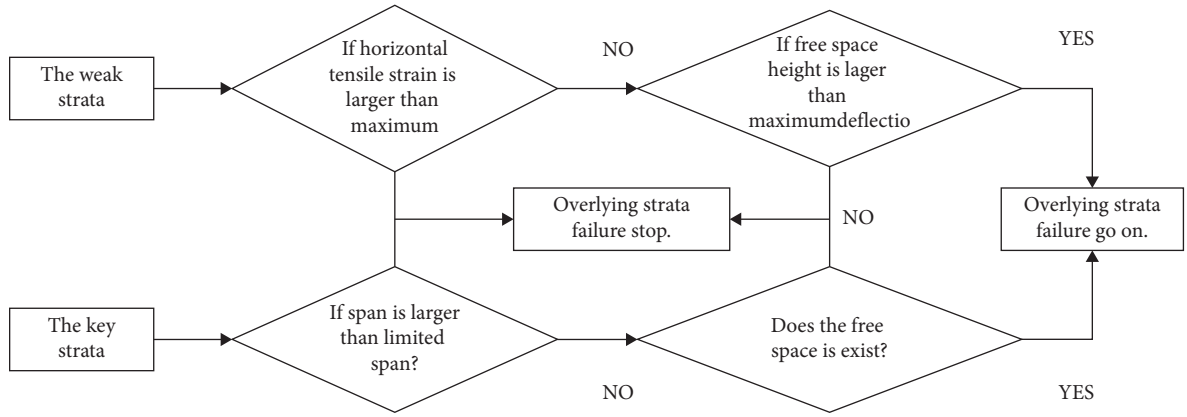

Figure 1: Judgment flow chart for height of fractured zone.

Table 2: Identification results of key strata.

No.	Lithological characters	Thickness (m)	Key strata	Failure span (m)	Distance from roof of coal seam (m)
Y25	Kernstone	25.4	Main key strata	104.18	174.6
Y22	Fine sandstone	10.7	Inferior key strata III	76.82	143.5
Y9	Fine sandstone	14.8	Inferior key strata II	67.44	32.4
Y2	K3 sandstone	5.3	Inferior key strata I	52.18	3.2

Table 3: Initial failure of each key strata with advancement of the working face.

Advancement of face (m)	Failure height of overlying strata (m)	Initial failure of key strata
55	32	Y2 (inferior key strata I)
109	143	Y9 (inferior key strata II)
193	174	Y22 (inferior key strata III)

strata fracture develops to the bottom of the main key strata, and overlying strata have a failure height of 174 m. As the face continues to advance, the fracture zone develops to the lower part of the main key strata, because the tendentious suspension and exposure span of the main key strata are less than its limit span.

4. Survey of Water Conducting Fractured Zone Height by Electromagnetic Image System

4.1. Survey Schemes. The EH4 continuous conductivity imaging system uses artificial emission signals to compensate for the deficiencies of certain frequency bands of natural signals to obtain high-resolution resistivity imaging.

EH4 electromagnetic imaging system was used in panel 8100 to classify the fractured and caved zones of the overburden by utilizing the different electrical conductivity characteristics of various strata. The survey was performed in three stages: (1) premining of intact overburden in May 2011; (2) postmining of mined-out gob in August 2011; and (3) postmining after movement of overburden had stabilized in May 2012. Two survey lines were laid out in panel 8100 (see Figure 2). Survey line #1 was located in area of panel 8100, where no mining would be performed, while survey line #2 was located above the gob of panel 8100. The length of survey line #1 was 160 m, containing nine measuring points. Survey line #2 was oriented at N21°W. It was 340 m long and contained 18 measuring points. In the second and third stages of surveys, survey was repeated along survey lines #1 and # 2. When the second stage of survey was performed, the panel had been mined out for one month. When the third stage of survey was performed, the panel had been mined out for 10 months.

4.2. Analysis of Survey Data. Figure 3 shows the two-dimensional Earth resistivity inversion of survey line #1 at each stage (double black dashed line is the seam position). According to the resistivity distribution, resistivity was higher, and there was little change in the area surrounded by red dotted line, and this area can be inferred to be a caving zone. The blue dashed line was the boundary of high and low resistivity, so the area between blue dashed line and red dotted line was a fracture zone. It can be seen from Figure 3(a) that the resistivity contours are smooth and continuous; there is little abnormal change of electrical conductivity density and no dislocation. The distribution of resistivity contours is layered except some fluctuations in shallow layers. The results confirmed that this area was not affected by coal mining, and the overburden was undisturbed. Similarly, it can be seen from Figure 3(b) that there were closed contour lines of abnormal electrical resistivity in an area bounded in the horizontal direction between 80 m and 180 m and in the vertical direction between +800 m and +880 m (the red dotted line). This abnormal area coincides

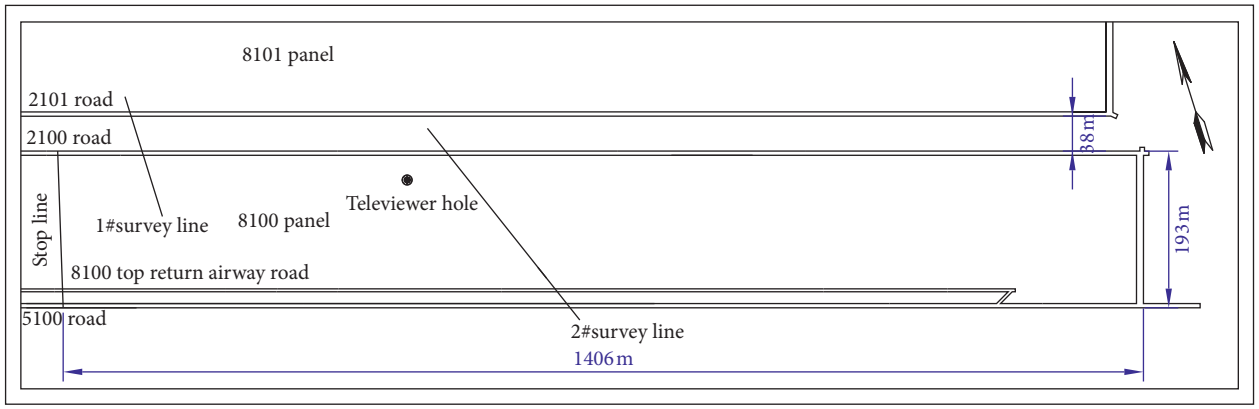

Figure 2: Panel layout.

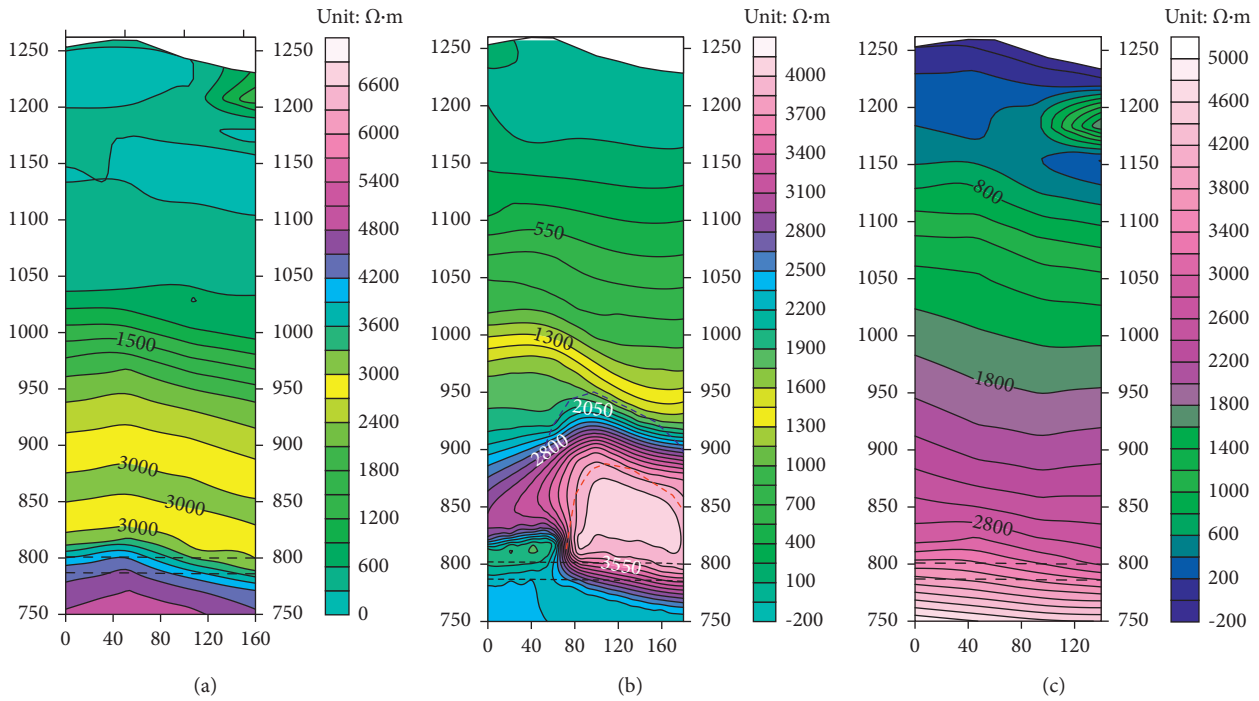

Figure 3: EH-4 two-dimensional inversion profiles of survey line #1. (a) The first stage (May 2011). (b) The second stage (August 2011). (c) The third stage (May 2012).

with the dimensions of panel 8100 shown in Figure 1. Therefore, it can be inferred that this high resistance anomaly area was the caved zone about 80 m high. The blue dashed line was the boundary of the fractured zone. It was about 150 m high. The continuous deformation zone covered the area from the boundary line of the fractured zone to ground surface. Again it can be seen from Figure 3(c) that high resistivity was distributed within a certain distance above the coal seam (double black dashed line is the seam position). Within this area, the resistivity contours were smooth, continuous, and layered, indicating that overburden movement had reached a steady state after one year of mining. Loose rocks and fractures are the cause of high electrical resistance. Resistivity contours are restored to the smooth layered distribution found in premining condition after overburden strata movement ceased and became compacted.

Figure 4 shows the two-dimensional earth resistivity inversion of survey line #2 at each stage (double black dashed line is the seam position). It can be seen from Figure 4(a) that there was a closed contour line bounded in the horizontal direction between 80 m and 300 m and in the vertical direction between +800 m and +900 m (the red dotted line). The abnormal area was matched with the dimensions of panel 8100 shown in Figure 1. Therefore, it can be inferred that this high resistance anomaly area was the caved zone about 100 m high. The blue dashed line was the boundary of the fractured zone. It was about 170 m high. The continuous

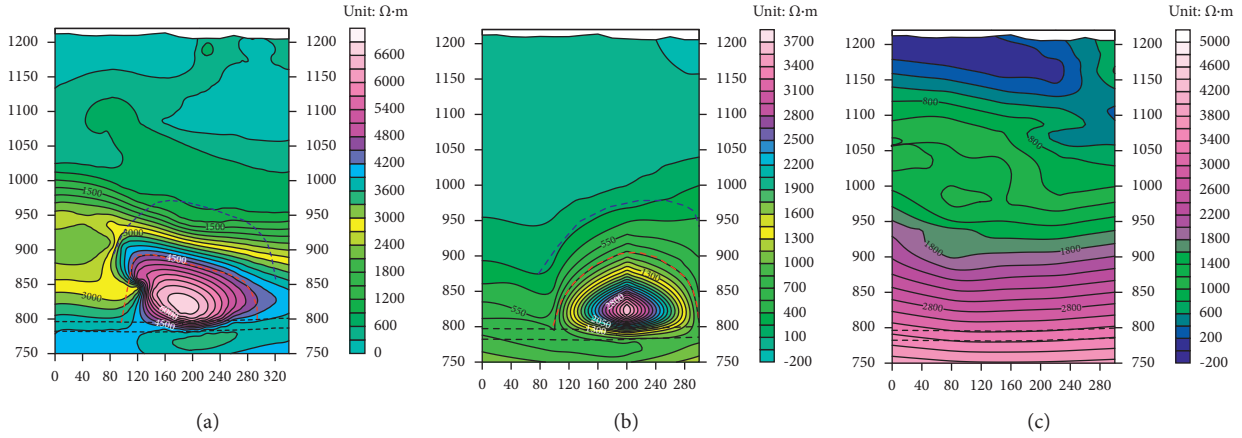

Figure 4: EH-4 two-dimensional inversion profiles of survey line #2. (a) The first stage (May 2011). (b) The second stage (August 2011). (c) The third stage (May 2012).

deformation zone covered the area from the boundary line of the fractured zone to the ground surface. The abnormal region in Figure 4(b) is consistent with the region in Figure 4(a). There was a closed contour line in the horizontal direction between 80 m and 300 m and in the vertical direction between +800 m and +900 m. So, it can be inferred that the caved zone is about 100 m high, and the fractured zone is about 170 m high. It can be seen from Figure 4(c) that resistivity contours were smooth, continuous, and layered, indicating that overburden movement had reached a steady state after one year of mining. Loose rocks and fractures are the cause of high electrical resistance. Resistivity contours are restored to the smooth layered distribution found in premining condition after overburden strata movement ceased and became compacted.

Table 4 is the summary of the EH4 geophysical survey results. The caved and fractured zones height at Tongxin mine was 150–170 m after mining of panel 8100 or 10 to 12 times of mining height (mining height = 15 m).

Table 4: EH4 survey results showing the height of the two zones in the gob.

Survey line	Caved zone height (m)	Fractured zone height (m)
1	80	70
2	100	70

5. Determination of Fractured Zone Height of Water Conductivity by Borehole Televiewer

The fractured zone height of water conductivity of panel 8100 was determined by using the JL-IDOI (A) Drilling TV Smart Imager (Figure 5) in July 2011. The surface borehole was located in the gob of panel 8100 about 456 m from the panel stop line. The distance between the borehole and 2100 transport road was 32 m (Figure 1). The vertical distance between borehole mouth and coal seam floor was 437.5 m, and the bottom end of the borehole was 60 m above the coal seam roof. The data collected by the borehole televiewer were used to analyze the fractures in various strata, and finally, the caved and fractured zones were determined.

Analysis of the images as viewed from the borehole televiewer indicated that the observation segments can be divided into four parts (Figure 6). The first part was the tiny fissure zone. It was 159–171 m from the coal seam floor. In this region, the fine sandstone is more or less intact with localized microcracks. This region was located within the

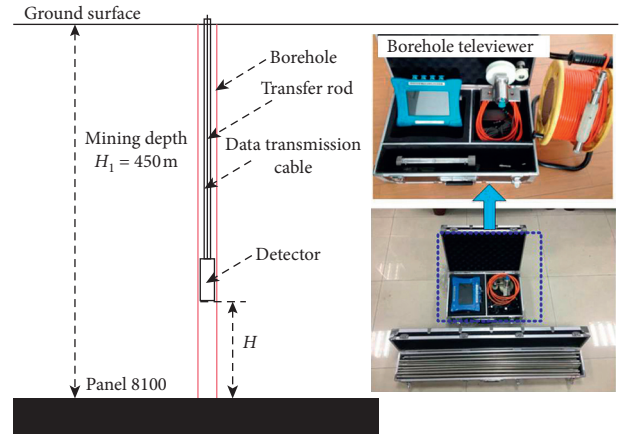

Figure 5: Borehole televiewer survey for roof strata.

fractured zone. The second part was the visible fractured zone, being located 90–159 m from the coal seam floor. There were visible crisscross cracks with bed separations. The third part was bed separation fractured zone, being located 60–90 m from the coal seam floor. In this region, broken rock, bed separation, and intact rocks alternated. This part bordered the caved zone. The fourth part was the badly broken zone, being located 0–60 m from the coal seam floor. Based on the above analysis, the caved zone height was about 90 m, that of the fractured zone was 81 m, and the height of overburden failures was 171 m (Figure 7).

In the ≪code for coal pillar setting and coal mining under pressure in buildings, water bodies, railways and main roadways≫, overlying failure height can be determined by

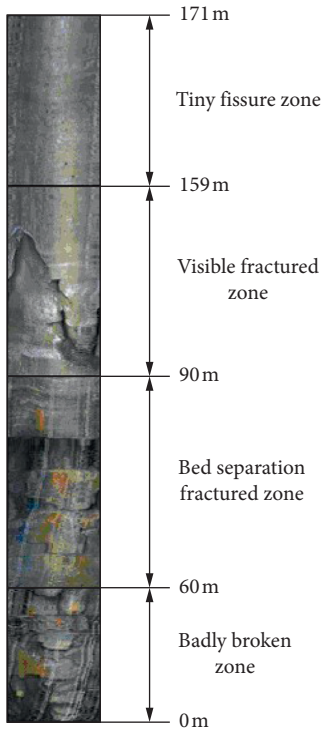

Figure 6: Damage characteristics of the hole wall.

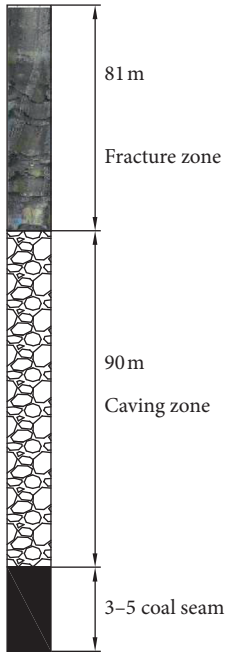

Figure 7: Caved and fractured zone heights.

(9) and (10) for thick coal seam under hard roof. The final calculation is based on the maximum value. Mining height is 15.3 m, and overlying failure heights are 66.25 m, 85.05 m, and 127.34 m calculated by (9) and (10). Therefore, overlying failure height was 127.34 m based on the code.

According to the above calculated results, the overburden failure height of the extra-thick coal seam was higher than that of the conventional thickness coal seam. It might be caused by the key strata.

$$H_{li} = \frac{100 \sum M}{1.2 \sum M + 2.0} \pm 8.9, \tag{9}$$

$$H_{li} = 30\sqrt{\sum M} + 10. \tag{10}$$

Table 5: Comparison of overlying failure height determined by different methods.

Methods	Overlying failure height (m)
Key strata theory	174
EH4 electromagnetic imaging system	150–170
Borehole televiewer	171
≪Code for coal pillar setting and coal mining under pressure in buildings, water bodies, railways and main roadways≫	127.34

Overlying failure heights determined by different methods are shown in Table 5. For theory calculation, EH4 electromagnetic imaging system, and borehole televiewer, the heights are nearly on the same level. So, the height of 170–174 m can be safely used. But the height calculated by the code is much lower than that of other methods. The equations proposed from many coal mines 20 years ago were outdated in the code, and the data was not complete for new mining methods, and new roof conditions and new mining height were applied in recent years.

The distance between panel 8100 in the No. 3–5 seam and the overlying No 14 seam was 190 m, more than the height of overburden failure zone. Therefore, cracks in the No. 3–5 seam did not connect to those in the No. 14 seam. The determination of the damage height of the overlying rock in the Tongxin Mine is of great significance to the prevention of mine water inrush accidents and gas control in the goaf of multiple coal seams and is beneficial to ensuring the safe production of the mine.

6. Conclusion

In China, there are few theories that can determine overlying failure height for thick and extra-thick coal seams. In order to understand the overburden movements of the longwall top coal caving mining, the key strata theory, EH4 geophysical survey, and borehole televiewer observation were applied to study this issue. The conclusions in this paper can be summarized as follows:

(1) The key strata controlling some overlying strata can affect overburden failure process. Applying key strata theory, the failure height was determined of 174 m.

(2) Through EH4 geophysical survey and borehole televiewer survey, the failure height was 150–171 m. The value is nearly the same as the key strata theory; therefore, the theory can be safely used for determination of overburden failure.

(4) The failure zone does not approach upper goaf, and the gas in the upper goaf will not threaten the mining of the 8100 working face. The determination of the damage height of the overlying rock in the Tongxin Mine is of great significance to the prevention of mine water inrush accidents and gas control in the goaf of multiple coal seams and is beneficial to ensuring the safe production of the mine.

Data Availability

No data were used in the study.

Conflicts of Interest

The authors declare no conflicts of interest.

Acknowledgments

This research has been supported by the Shandong Province Deep Rock Burst Disaster Assessment Engineering Laboratory Open Project (LMYK2021001) and Liaoning Revitalization Talents Program (XLYC1807064).

References

[1] L. M. Dou, J. He, S. Gong, and Y. F. Song, "A case study of micro-seismic monitoring: goaf water-inrush dynamic hazards," *Zhongguo Kuangye Daxue Xuebao/Journal of China University of Mining and Technology*, vol. 41, no. 1, pp. 20–25, 2012.

[2] M. H. Loke, J. E. Chambers, D. F. Rucker, O. Kuras, and P. B. Wilkinson, "Recent developments in the direct-current geoelectrical imaging method," *Journal of Applied Geophysics*, vol. 95, pp. 135–156, 2013.

[3] B. Poulsen, M. Khanal, A. M. Rao, D. Adhikary, and R. Balusu, "Mine overburden dump failure: a case study," *Geotechnical & Geological Engineering*, vol. 32, no. 2, pp. 297–309, 2014.

[4] W. Liu, L. Pang, B. Xu, and X. Sun, "Study on overburden failure characteristics in deep thick loose seam and thick coal seam mining," *Geomatics, Natural Hazards and Risk*, vol. 11, no. 1, pp. 632–653, 2020.

[5] X. Wang, Q. Qin, and C. Fan, "Failure characteristic and fracture evolution law of overburden of thick coal in fully mechanized sub-level caving mining," *Sains Malaysiana*, vol. 46, no. 11, pp. 2041–2048, 2017.

[6] M. van Schoor, "The application of in-mine electrical resistance tomography (ERT) for mapping potholes and other disruptive features ahead of mining," *Journal of the South African Institute of Mining and Metallurgy*, vol. 105, no. 6, pp. 447–451, 2005.

[7] A. Kidybinski and C. O. Babcock, "Stress distribution and rock fracture zones in the roof of longwall face in a coal mine," *Rock Mechanics*, vol. 5, no. 1, pp. 1–19, 1973.

[8] V. Palchik, "Formation of fractured zones in overburden due to longwall mining," *Environmental Geology*, vol. 44, no. 1, pp. 28–38, 2003.

[9] K. W. Mills, O. Garratt, B. G. Blacka, L. C. Daigle, A. C. Rippon, and R. J. Walker, "Measurement of shear movements in the overburden strata ahead of longwall mining," *International Journal of Mining Science and Technology*, vol. 26, no. 1, pp. 97–102, 2016.

[10] M. Ju, X. Li, Q. Yao, S. Liu, S. Liang, and X. Wang, "Effect of sand grain size on simulated mining-induced overburden failure in physical model tests," *Engineering Geology*, vol. 226, pp. 93–106, 2017.

[11] B. Y. Sun, P. S. Zhang, R. X. Wu, and L. Q. Guo, "Dynamic detection and analysis of overburden deformation and failure in a mining face using distributed optical fiber sensing," *Journal of Geophysics and Engineering*, vol. 15, no. 6, pp. 2545–2555, 2018.

[12] D. Yang, W. Guo, and Y. Tan, "Application of magnetotelluric method to the detection of overburden failure height in shallow seam mining," *Arabian Journal of Geosciences*, vol. 11, no. 13, 2018.

[13] R. H. Chen, H. B. Bai, and M. M. Feng, "Determination of the height of water flowing fractured zone in overburden strata above fully-mechanized top-coal caving face," *Journal of Mining & Safety Engineering*, vol. 23, no. 2, pp. 220–223, 2006.

[14] H. Wang, "Research on microseism monitor in height of water flowing fractured zone of cover rock," *Express Information of Mining Industry*, no. 3, pp. 27–29, 2006.

[15] H. Wang, Y. Qin, H. Wang, Y. Chen, and X. Liu, "Process of overburden failure in steeply inclined multi-seam mining: insights from physical modelling," *Royal Society Open Science*, vol. 8, no. 5, Article ID 210275, 2021.

[16] Z. Xu, Q. Li, and X. Li, "Overburden migration and failure characteristics in mining shallow buried coal seam with thick loose layer," *Advances in Materials Science and Engineering*, vol. 2020, Article ID 9024751, 12 pages, 2020.

[17] L. Pang, W. Liu, and Y. Qin, "Analysis of main controlling factors of overburden failure in coal mining under thick coal seam geological conditions," *Geotechnical & Geological Engineering*, vol. 39, no. 4, 2020.

[18] D. Yang, W. Guo, and Y. Tan, "Study on the evolution characteristics of two-zone failure mode of the overburden strata under shallow buried thick seam mining," *Advances in Civil Engineering*, vol. 2019, Article ID 9874769, 9 pages, 2019.

[19] J. Ju and J. Xu, "Structural characteristics of key strata and strata behaviour of a fully mechanized longwall face with 7.0m height chocks," *International Journal of Rock Mechanics and Mining Sciences*, vol. 58, pp. 46–54, 2013.

[20] J. Xu, W. Zhu, and X. Wang, "New method to predict the height of fractured water-conducting zone by location of key strata," *Journal of China Coal Society*, vol. 37, no. 5, pp. 762–769, 2012.

[21] Y. Yuan, S. Tu, X. Zhang, and B. Li, "Dynamic effect and control of key strata break of immediate roof in fully mechanized mining with large mining height," *Shock and Vibration*, vol. 2015, Article ID 657818, 11 pages, 2015.

[22] T. Kuang, Z. Li, W. Zhu et al., "The impact of key strata movement on ground pressure behaviour in the Datong coalfield," *International Journal of Rock Mechanics and Mining Sciences*, vol. 119, pp. 193–204, 2019.

[23] H. Han, J. Xu, X. Wang, J. Xie, and Y. Xing, "Method to calculate working surface abutment pressure based on key strata theory," *Advances in Civil Engineering*, vol. 2019, Article ID 7678327, 20 pages, 2019.

[24] K. Wang, T. Kang, H. Li, and W. Han, "Study of control caving methods and reasonable hanging roof length on hard roof," *Chinese Journal of Rock Mechanics and Engineering*, vol. 28, no. 11, pp. 2320–2327, 2019.

[25] X. J. Lin and M. G. Qian, "Method to distinguish key strata in overburden," *Journal of China University of Mining & Technology*, vol. 29, 2000.

[26] J. Cheng, G. Zhao, and S. Li, "Predicting underground strata movements model with considering key strata effects," *Geotechnical and Geological Engineering*, vol. 36, 2017.

[27] C. Xu, G. Yang, H. Sun et al., "Key strata inducing dynamic disasters based on energy condition: criterion and application," *Geofluids*, vol. 2021, Article ID 6672020, 10 pages, 2021.

[28] W. Lu, C. He, and X. Zhang, "Height of overburden fracture based on key strata theory in longwall face," *PLoS One*, vol. 15, Article ID e0228264, 2020.